VascularBiology

Vascular Biology (2025) **7** e250001
https://doi.org/10.1530/VB-25-0001

Received 18 March 2025
Accepted 7 May 2025
Available online 7 May 2025
Version of Record published 20 May 2025

RESEARCH

Lipocalin 2 deficiency impacts angiogenesis after ischemia *in vivo* and *in vitro*

L Zhang[1,2,*], Z Aref[1,2,*], H A B Peters[1,2], M R de Vries[1,2], A Y Nossent[3] and P H A Quax[1,2]

[1]Einthoven Laboratory for Experimental Vascular Medicine and Regenerative Medicine, Leiden University Medical Center, Leiden, The Netherlands
[2]Department of Surgery, Leiden University Medical Center, Leiden, The Netherlands
[3]Department of Nutrition, Exercise and Sports, University of Copenhagen, Copenhagen, Denmark

Correspondence should be addressed to P H A Quax: p.h.a.quax@lumc.nl

*(L Zhang and Z Aref contributed equally to this work)

Abstract

Therapeutic neovascularization is a promising therapy option for patients with peripheral arterial disease. We followed in time the gene expression after induction of hind limb ischemia in mice with different patterns of blood flow restoration and identified lipocalin 2 (LCN2) as a strongly upregulated factor whose role in neovascularization deserves further investigation. In this study, we investigated the role of LCN2 in angiogenesis using the hind limb ischemia (HLI) model, *ex vivo* angiogenic aortic ring assay, and by assessing the pre-existing collaterals in the pial circulation in both *Lcn2*$^{-/-}$ mice and wild-type (WT) mice. This demonstrated an upregulated mRNA expression of *Lcn2* after HLI and reduced post-ischemic angiogenesis in *Lcn2*$^{-/-}$ compared to WT mice. In the aortic ring assay, angiogenic sprouting was decreased in *Lcn2*$^{-/-}$ compared to WT mice. The blood flow recovery and arteriogenesis after HLI and preexisting collateral density in the pial circulation were similar in *Lcn2*$^{-/-}$ and WT mice. *In vitro*, siRNA-mediated *LCN2* knockdown impaired HMVEC migration and tube formation. These results show that LCN2 is a potential pro-angiogenic factor and that LCN2 downregulation has a negative effect on angiogenesis *in vivo* and *in vitro*.

Keywords: lipocalin 2; LCN2; angiogenesis; peripheral arterial disease; endothelial cell; microvasculature

Introduction

Peripheral arterial disease (PAD) is a major cause of morbidity and mortality (1). PAD is caused by atherosclerosis in blood vessels in the limbs, which leads to reduced blood flow through the legs. The current medical treatment of PAD includes conventional percutaneous and/or surgical revascularization. However, many patients have recurrent complaints about restenosis after these treatments. In addition, some patients are poor candidates for these endovascular and surgical approaches due to comorbidities or anatomical restrictions. For these poor responders and patients who are not suitable for vascular intervention approaches, therapeutic neovascularization is a promising alternative approach.

Therapeutic neovascularization includes induction of angiogenesis and arteriogenesis since these two mechanisms both participate in compensating the consequences of arterial occlusion. Angiogenesis is the process of sprouting new capillaries from pre-existing microvasculature and is driven by ischemia. Ischemia leads to the activation of, among others, hypoxia-inducible transcription factors (HIFs), and this induces the expression of angiogenic genes, including VEGF-A (2). Inflammatory cells are also important for angiogenesis (3), as they contribute by secreting cytokines and chemokines that may affect endothelial functions.

Arteriogenesis is the outward remodeling of collateral arteries from the pre-existing arteriole network.

Published by Bioscientifica Ltd.
https://vb.bioscientifica.com

Vascular Biology (2025) **7** e250001
https://doi.org/10.1530/VB-25-0001

Arteriogenesis is triggered by increased shear stress against the arteriole wall, which leads to the activation of endothelial cells such that these cells then express adhesion molecules and secrete chemokines and inflammatory cytokines (4). This leads to the induction of an inflammatory response and recruitment of leukocytes, including neutrophils (5). The clinical trials, which targeted vascular remodeling with the obvious potential targets (such as vascular endothelial growth factor (VEGF), fibroblast growth factor, or hepatocyte growth factor) acquired from animal research, have shown disappointing results (6, 7, 8, 9). Therefore, further research is required to find factors that are involved in neovascularization, including both arteriogenesis and angiogenesis, and may provide new therapeutic possibilities.

In mice, post-ischemic blood flow recovery patterns differ for each strain of mice based on their genetic background (10). The biggest difference is seen between C57BL/6 and Balb/c mice, whereby C57BL/6 mice show the best blood flow recovery, and Balb/c mice show the poorest. C57BL/6 mice have more pre-existing collateral arteries and a good remodeling capacity after induction of ischemia (11). Balb/c mice have no preexisting collateral arteries in the pial circulation and only a few in the intestine. The skeletal muscles of Balb/c mice show an altered pattern of the preexisting collateral arteries. Furthermore, after induction of ischemia, Balb/c mice show a hampered remodeling response (10, 12, 13). In a previous study in which we compared C57BL/6 and Balb/c mice (14), we found a multitude of differences in immune regulatory genes and found *Lcn2* as the highest upregulated. This finding provides us with a new target for therapeutic neovascularization.

The *Lcn2* gene encodes lipocalin 2 (LCN2) protein. LCN2 is also known as 24p3 in mice and as neutrophil-gelatinase-associated lipocalin (NGAL) in humans. LCN2 is a 25 kDa protein that was originally found in the granules of neutrophils (15). Later research showed that other cell types also release LCN2 in response to various injuries (16, 17). LCN2 mediates an innate immune response to bacteria by iron sequestration (18). In mice, LCN2 is associated with atherosclerosis in a stage-dependent manner (19). LCN2/NGAL was increased in atherosclerotic plaques in mice and humans (20), especially in unstable plaques in humans (21). In addition, clinical studies showed that serum levels of NGAL were higher in patients with coronary artery disease (CAD) compared to healthy controls (22). These studies also showed that patients with acute myocardial infarction had higher levels of NGAL compared to patients with stable CAD (23). Besides serum changes, LCN2/NGAL was also detected in patients with PAD, in human femoral plaques in regions rich in inflammatory cells, and increased serum levels of LCN2 were associated with an increased risk for cardiovascular events in PAD patients (24).

LCN2 is an acute-phase inflammatory protein and is upregulated via different pro-inflammatory factors and may enhance the atherosclerotic process, leading to increased cardiovascular risks (25). As intraplaque angiogenesis is also an important factor in atherosclerotic lesion development (26) and in rat brain endothelial cells, LCN2 enhanced angiogenesis via iron and ROS-related pathways (27), it is unclear what the exact role of LCN2 in PAD is. Previous research reported that LCN2 is involved in inflammation, which is crucial for neovascularization, although it remained unclear whether this relates to arteriogenenesis, angiogenesis, or both. Therefore, we hypothesize that LCN2 plays a role in neovascularization. However, whether this relates more to arteriogenesis/collateral formation or more to angiogenesis remains to be determined.

To this end, we investigated the role of LCN2 in neovascularization *in vivo* using the hind limb ischemia model and the *ex vivo* aortic ring assay in *Lcn2* knockout mice, which showed that angiogenesis, but not arteriogenesis, was affected. To confirm these findings, human microvascular endothelial cells (HMVECs) were used to investigate the effect on *in vitro* angiogenesis after *LCN2* knockdown using siRNAs.

Materials and methods

Animals

All animal experiments were performed in compliance with Dutch government guidelines and the Directive 2010/63/EU of the European Parliament and approved by the committee on animal welfare of the Leiden University Medical Center (The Netherlands). *Lcn2*$^{-/-}$ mice were kindly made available by Professor T W Mak from the University Health Network in Canada (28). Male C57BL/6 and *Lcn2* knockout mice from the age of 8–12 weeks were used in these experiments and received a high-fat cholesterol-rich diet.

In vivo murine hind limb ischemia model

Hind limb ischemia was induced in C57BL/6 and *Lcn2*$^{-/-}$ mice. Mice were anesthetized by intraperitoneal injection of a mixture of midazolam (8 mg/kg), medetomidine (0.4 mg/kg), and fentanyl (0.08 mg/kg). Subsequently, surgical unilateral induction of hind limb ischemia was accomplished by electro-coagulation of the left common femoral artery proximal to the bifurcation of the superficial and deep femoral arteries.

To analyze the blood flow in the tissue, Laser Doppler perfusion imaging (LDPI) (Moor Instruments, UK) analysis was performed. Mice were anesthetized with intraperitoneal injection of midazolam (8 mg/kg) and medetomidine (0.4 mg/kg) before the measurements.

Vascular Biology (2025) **7** e250001
https://doi.org/10.1530/VB-25-0001

LDPI was performed before, immediately after, and on the day 7, 10, 14, 21, and 28 after induction of ischemia. Perfusion measurements were obtained by the ratio of ischemic to non-ischemic paw. After each measurement, anesthesia was antagonized with flumazenil (0.7 mg/kg) and atipamezole (3.3 mg/kg), except for the final measurement at day 28, when mice were sacrificed directly after LDPI measurements when still under anesthesia and with additional fentanyl (0.08 mg/kg) painkilling (29).

RNA isolation and whole-genome expression profiling

To unravel the gene pattern after HLI in C57BL/6 mice, whole-genome expression profiling was performed. Mice were killed under anesthesia before and at different time points after induction of HLI (days 1, 3, 7, 14, and 28), and the adductor muscle group was removed. The tissue of the adductor muscle was snap-frozen, crushed, and homogenized over a Qiashredder (Qiagen, Germany). Total RNA was isolated from the tissue or cells by using an RNeasy Fibrous Tissue Mini Kit (Qiagen), and RNA integrity was checked by NanoDrop (ThermoFisher, USA) and Bioanalyzer (Agilent Technologies, USA).

For array analysis, MouseWG-6 v2.0 Expression BeadChips (Illumina, USA) were used, and statistical analysis of microarray data (SAM) was used for analysis as described by Nossent *et al.* (14).

Real-time quantitative PCR

We performed real-time quantitative PCR to validate the data of array analysis and to confirm the *Lcn2* level after siRNA transfection. RNA was reverse transcribed using a High-Capacity RNA-to-cDNA Kit (Applied Biosystems, ThermoFisher, USA). For murine samples, quantitative PCR was performed on the ABI 7500 fast system, using commercially available TaqMan gene expression assays for murine *Lcn2* (Applied Biosystems). CT values were normalized against *Hprt1*. For HMVECs, quantitative PCR was performed by SYBR Green reagents (Qiagen) on the QuantStudio™ 5 System (Applied Biosystems), and CT values were normalized against GAPDH.

Preexisting collateral density

Mice were anesthetized with midazolam (8 mg/kg), medetomidine (0.4 mg/kg), and fentanyl (0.08 mg/kg) and heparinized. The thoracic aorta was cannulated retrograde, and the circulation was maximally dilated by infusion of sodium nitroprusside (30 μg/mL) and papaverine (40 μg/mL) in PBS at approximately 100 mmHg before vascular casting. After craniotomy, yellow Microfil (Flow Tech Inc., USA) was infused under a stereomicroscope. The dorsal cerebral circulation was fixed with a topical application of 4% paraformaldehyde (PFA) to prevent any degradation in vessel dimensions after Microfil injection. The brains were fixed overnight in 4% PFA and were subsequently incubated in Evans Blue (2 μg/mL in 4% PFA) for several days to improve contrast for visualization of the vasculature. Digital images were acquired of the dorsal brain surface and processed with ImageJ software (NIH). Collateral density was calculated by determining the total number of pial collaterals between the anterior cerebral artery (ACA)-middle cerebral artery (MCA), ACA-posterior cerebral artery (PCA), and MCA-PCA, divided by the dorsal surface area of the cerebral hemispheres. Uncountable areas due to tissue damage or incomplete filling were excluded from the analysis (10, 30, 31).

Immunohistochemistry

For harvesting tissues, mice were anesthetized by intraperitoneal injection of a mixture of midazolam (8 mg/kg), medetomidine (0.4 mg/kg), and fentanyl (0.08 mg/kg). Subsequently, mice were sacrificed by exsanguination.

Mice were sacrificed under anesthesia 10 days after induction of HLI. The adductor and gastrocnemius muscles from the ligated and non-ligated limbs of both *Lcn2*$^{-/-}$ and WT mice were harvested. The adductor muscle group was fixed in 4% PFA, and immunohistochemical analysis was performed on paraffin sections (5 μm) of muscles of both the ligated and non-ligated limbs of both groups. To detect the collateral arterioles, sections of the adductor group muscle were stained with anti-smooth muscle α-actin (anti-αSMA, Dako). The sections were counterstained with hematoxylin. The lumen diameter and number of αSMA-positive vessels were quantified using ImageJ software.

The gastrocnemius muscle was snap-frozen in liquid nitrogen after harvesting. Frozen sections (5 μm) of the ligated and non-ligated limbs of both groups were fixed in ice-cold acetone and stained with anti-CD31 (Santa Cruz Biotechnology, USA), followed by a secondary anti-rabbit antibody conjugated with Alexa 488 fluorochrome (Molecular Probes). Vectashield with DAPI (Vector Laboratories, USA) was used to stain the cell nuclei. Staining was quantified from fluorescent images taken using an LSM700 microscope (Carl Zeiss, Germany) and contrast-stretched using Zen 2009 software (Carl Zeiss) (32).

Murine aortic ring assay

Mouse aortic ring assays were performed as previously described (33). Briefly, the thoracic aorta was removed from WT and *Lcn2* $^{-/-}$ mice and transferred to a petri dish containing Opti-MEM (Gibco, ThermoFisher, USA). The surrounding branching vessels and fat were gently removed, and the aorta was flushed with Opti-MEM

Vascular Biology (2025) **7** e250001
https://doi.org/10.1530/VB-25-0001

(Gibco). Aortic rings of 0.5–1 mm were transported to fresh Opti-MEM with antibiotics and serum-starved overnight. Collagen (type I, Millipore, MilliporeSigma, USA) was diluted to a concentration of 1 mg/mL with 1xDMEM (Gibco) and the pH was adjusted with 5N NaOH. Ninety-six-well plates were coated with 70 μL collagen matrix. Rings were transported into the wells, and after 1 h, 150 μL Opti-MEM supplemented with 2.5% fetal bovine serum (FBS) (PAA, Austria), penicillin-streptomycin (PAA, Austria), and 30 ng/mL VEGF was added to each well. The medium was changed first on day 3. Microvessel outgrowth was quantified after 7 days by live phase-contrast microscopy (Axiovert 40C, Carl Zeiss). Each microvessel emerging from the ring was counted as a sprout, and individual branches arising from each microvessel were counted as separate sprouts.

Primary HMVECs cell culture

Human microvascular endothelial cells (HMVECs), derived from the foreskin, were cultured at 37°C in a humidified 5% CO_2 environment with HMVECs culture medium (EBM-2 basal medium (CC-3156)) containing 10% FBS and EGMTM-2 (Single Quots™ Supplements (CC-4176), Lonza, Switzerland). Medium was refreshed every 2–3 days. Cells were passed using trypsin (Sigma, USA) at 70–80% confluency.

LCN2 knockdown with siRNA transfection *in vitro*

Primary HMVECs were seeded in 12-well plates coated with 1% fibronectin at 100,000 cells per well in the HMVECs culture medium to establish subconfluent cultures. After 24 h, cells were washed with PBS, and each well was incubated with 900 μL culture medium and 100 μL of transfection medium (94 μL culture medium with 3 μL of Lipofectamine RNAiMax (Life Technologies, the Netherlands) and 3 μL of siRNA, incubated for 10 min). The final siRNA concentration per well was 30 nM. The siRNA used was siRNA-LCN2 (AM51331). After the addition of transfection agents, cells were incubated at 37°C for 48 h according to the manufacturer's protocol.

Migration assay–scratch wound healing

Primary HMVECs were seeded in 12-well plates coated with 1% fibronectin at 120,000 cells per well in the HMVECs culture medium to establish confluent cultures. After 24 h, the medium was replaced with the transfection medium as previously described. Then, transfection was conducted, and a scratch wound was performed across the diameter of each well by using a p200 pipette tip for each well. Next, cells were washed with PBS and incubated in the starving medium (EBM-2 (Lonza) containing only 1% FBS and 1% gentamicin-amphotericin of the provided BulletKit). To monitor scratch-wound closure, live phase-contrast microscopy (Axiovert 40C, Carl Zeiss) was used for taking pictures at 24 and 36 h after introducing the scratch wound. Pictures were taken in the same location at two positions in each well. Scratch size was calculated using the wound healing tool macro for ImageJ. Each single scratch assay condition was performed in triplicate, and the scratch-wound healing assay was repeated three times.

Tube-formation assay

Tube-formation assay was performed using HMVECs. At 90% confluence, cells were transfected as described above with Lipofectamine RNAiMax and siRNA-LCN2, or siRNA negative control. After 24 h, cells were counted and seeded in a 96-well plate at 15,000 cells per well. Plates were coated with Geltrex™ (ref: A14132-02, Gibco) for 30 min before seeding. Photos were taken using live phase-contrast microscopy at 12 h after seeding and quantified using the ImageJ. Each single tube-formation assay was performed in six wells per condition, and the tube-formation assay was performed three independent times. The number of segments, the number of branches, and the total length of the branches were analyzed with ImageJ.

MTT assay

HMVECs were seeded in a 96-well plate coated with 1% gelatin at 5,000 cells per well with culture medium, six wells per condition. After 24 h, the medium was replaced with starve medium (EBM-2 (Lonza) containing only 0.2% FBS and 1% gentamicin-amphotericin of the provided Bullet Kit) for another 24 h. Then, for the transfection group, cells were cultured with transfection medium as previously described, containing lipofectamine with siRNA-LCN2 or siRNA negative control. For control groups, cells treated with culture medium containing 20% DMSO were used as the negative control, and cells treated with culture medium were used as the positive control. Six blank wells were filled with culture medium as blank control. After 44 h of transfection, 10 μL of 5% MTT (thiazolyl blue tetrazolium bromide, Sigma M5655) was added directly to each well in each group and incubation was continued at 37°C, 5% CO_2, for 4 h. Absorbance at 590 nm was measured using a Cytation 5 spectrophotometer (BioTek, USA).

Statistical analysis

Data are presented as the mean ± SEM. Indicated differences had the following levels of significance: $^{*}P < 0.05$, $^{**}P < 0.01$, $^{***}P < 0.001$, $^{****}P < 0.0001$. All tests were performed with a significance level of $\alpha = 0.05$. Independent sample Student's *t*-tests and one-way ANOVA tests were performed depending on different experiment settings, which will be described in the figure legends.

Vascular Biology (2025) **7** e250001
https://doi.org/10.1530/VB-25-0001

Results

Upregulated mRNA expression level of *Lcn2* after HLI

To identify factors that are essential in post-ischemic blood flow recovery, we determined gene expression profiles in C57BL/6 mice. The recovery of perfusion in C57BL/6 mice is more rapid than in Balb/c after HLI (34), which makes it interesting to know which genes are most upregulated in C57BL/6 mice and may induce vascular remodeling.

In this study, 3.729 genes in C57BL/6 mice were significantly up- or downregulated over time, whereas 786 genes were already upregulated at day 1 after induction of HLI. The gene that was significantly highest upregulated on day 1 after induction of HLI in the adductor muscle was *Lcn2* (Significance Analysis of Micro Data (SAM), q < 5%); after day 1 the expression dropped. In the model of HLI, angiogenesis occurs mainly in the gastrocnemius muscle, where the ischemia takes place, and arteriogenesis occurs mainly in the adductor muscle. To validate the data of the array analysis and to determine the expression of *Lcn2* in the ischemic area, we performed real-time PCR and quantified the expression level of *Lcn2* in the left (the ligated side) adductor muscle and in the left gastrocnemius muscle of C57BL/6 mice (Fig. 1A, B, C, D).

Arteriogenesis in *Lcn2*$^{-/-}$ mice

To investigate the role of LCN2 in neovascularization, we studied blood flow recovery after HLI in *Lcn2*$^{-/-}$ mice compared with WT mice. The functional blood perfusion was measured by Laser Doppler perfusion imaging and showed the same amount of restoration of blood flow after HLI in both strains, leading to a rapid induction of the recovery with flow ratios more than 0.5 at 10 days and full recovery of the flow after 28 days (Fig. 2A and B).

To rule out the influence of preexisting collateral density differences on arteriogenesis, the number of collaterals in the pial circulation of both strains was assessed. Preexisting collateral density in the pial circulation of the dorsal cerebral cortex predicts collateral density in skeletal muscle (10, 30). Preexisting collateral density was similar between *Lcn2*$^{-/-}$ and WT mice (Fig. 2D and E, P = 0.16), which was in accordance with a decrease in paw perfusion directly after induction of HLI in both WT and *Lcn2* $^{-/-}$ mice (Fig. 2C, P = 0.19). Even though the number of preexisting collaterals was similar, and the paw perfusion in the ischemic and non-ischemic paw after induction was similar in both strains, the collateral lumen area was increased after ischemia in *Lcn2*$^{-/-}$ mice, since the ratio of collateral lumen area between ligated limb and unligated limb is above 1 (Fig. 2H). However, there was no significant difference in the histological analysis

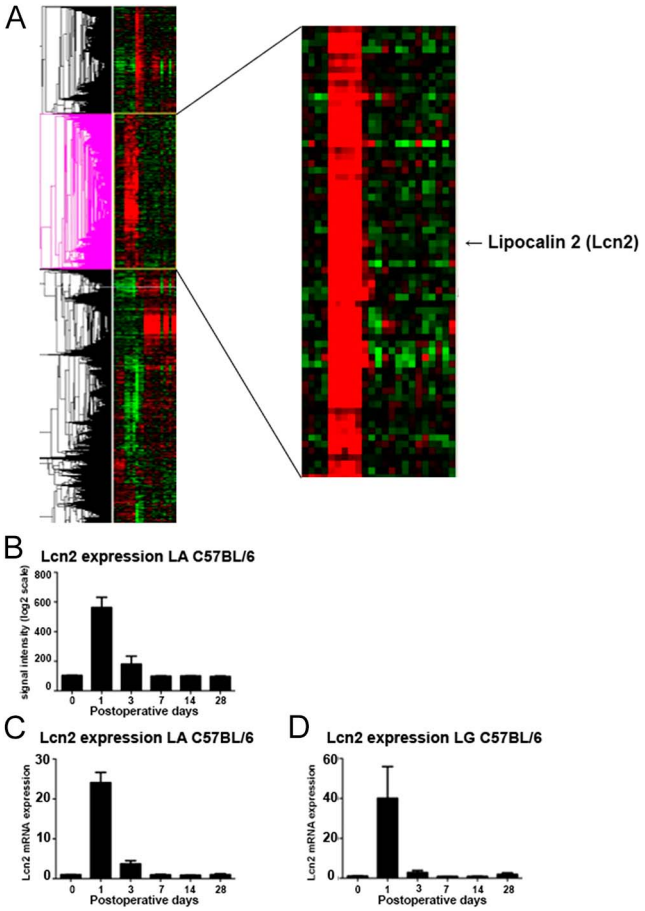

Figure 1

Lcn2 expression in the HLI model (A) heatmap of gene regulation before and after induction of HLI in C57BL/6 mice (n = 3). The pink-colored lines show genes that are significantly upregulated on day 1 after induction of HLI. n, number of mice. (B) Array signal of *Lcn2* expression in the adductor muscle of C57BL/6 mice (n = 3) before and after induction of HLI. LA, left adductor. (C) *Lcn2* mRNA expression in left adductor muscles of C57BL/6 mice (n = 3) before inducing HLI and after, as measured by RT-qPCR. (D) *Lcn2* mRNA expression in left gastrocnemius muscles of C57BL/6 mice (n = 3) before and after inducing HLI, as measured by RT-qPCR. LG, left gastrocnemius. Data are presented as mean ± SEM.

of collateral size and number in the *Lcn2*$^{-/-}$ mice compared to WT mice after ischemia (Fig. 2F, G, H).

Angiogenesis in *Lcn2*$^{-/-}$ mice

To assess the effect of *Lcn2* deficiency on ischemia-driven angiogenesis, the numbers of capillaries, as well as the average size of capillaries, were quantified in both ischemic and non-ischemic gastrocnemius muscles (Fig. 3A). The *Lcn2*$^{-/-}$ mice showed a decrease of 18% (P < 0.05) in capillary density (Fig. 3B) and of 25% (P < 0.001) in the capillary size (Fig. 3C) in the ischemic paw as compared to WT mice. As reduced post-ischemic angiogenesis was observed *in vivo* in *Lcn2* $^{-/-}$

Vascular Biology (2025) **7** e250001
https://doi.org/10.1530/VB-25-0001

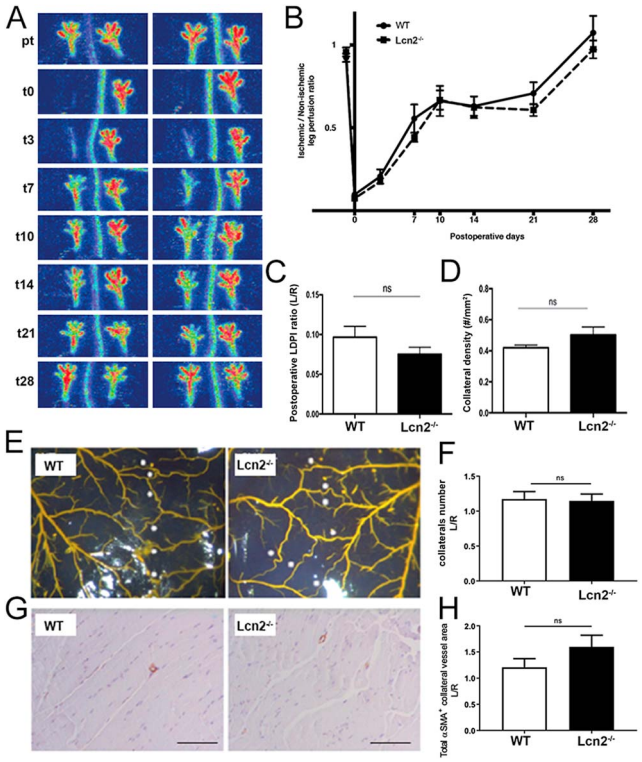

Figure 2

Blood flow recovery and pre-existing collateral bed in *Lcn2*$^{-/-}$mice (A) representative Laser Doppler perfusion imaging (LDPI) images of paws from WT and *Lcn2* $^{-/-}$ mice after induction of HLI in the left limb. (B) Quantification of LDPI measurements of *Lcn2*$^{-/-}$ (n = 10) and WT (n = 9) mice over time. Data are calculated as the ratio of ligated to non-ligated paws. n, number of mice. (C) Quantification of LDPI measurements of *Lcn2*$^{-/-}$ and WT directly after induction of HLI. (D) Pial collateral density was calculated in WT and *Lcn2* $^{-/-}$ mice. (E) Representative images of the pial circulation in WT and *Lcn2*$^{-/-}$ mice. White asterisks indicate collateral arteries between the anterior, middle, and posterior cerebral arteries (ACA, MCA, and PCA, respectively). (G) Immunohistochemical staining of paraffin-embedded adductor muscle of WT (n = 9) and *Lcn2* $^{-/-}$ (n = 10) mice, using anti-αSMA (red) antibodies. The scale bar represents 100 μm. (F) and (H) The ratio of αSMA^{+} vessel numbers and the lumen areas between ligated (left) and non-ligated (right) limbs in the adductor muscle. Data were analyzed using independent sample Student's *t*-tests and are presented as mean ± SEM. ns, no significant difference.

mice after HLI, we further performed an *ex vivo* angiogenic aortic ring assay to determine sprout formation *ex vivo*. The quantified average number of sprouts (Fig. 4) and angiogenic sprouting was significantly decreased in *Lcn2* $^{-/-}$ compared to WT mice (by 61%, P = 0.0052).

LCN2 knockdown *in vitro*

To study the role of LCN2 *in vitro*, human microvessel endothelial cells (HMVECs) were transfected with small interfering RNA (siRNA) targeted to *LCN2*, of which

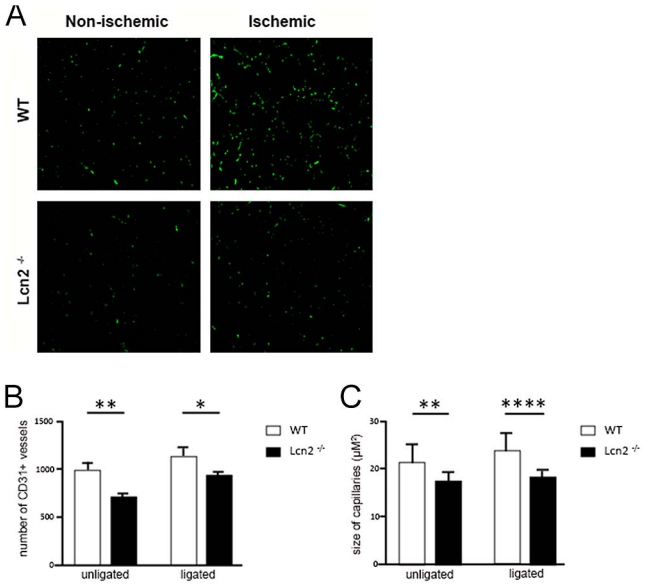

Figure 3

Angiogenesis *in vivo*. (A) Representative images of CD31 staining in the right (non-ischemic) and left (ischemic) soleus muscles of WT (n = 9) and *Lcn2* $^{-/-}$(n = 10) mice. n: number of mice. (B) Capillary density in soleus muscles is defined as the number of CD31+ vessels per section. (C) Capillary size in gastrocnemius muscles of WT and *Lcn2* $^{-/-}$ mice. Data were analyzed using independent sample Student's *t*-tests and are presented as mean ± SEM, *P < 0.05, **P < 0.01, ****P < 0.0001.

angiogenesis function was assessed with scratch assay, MTT assay, and tube formation. HMVECs were treated with lipofectamine as the control in the following angiogenesis experiments.

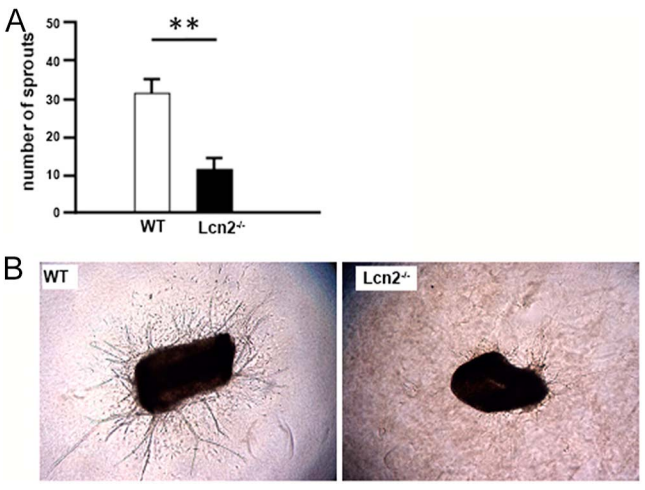

Figure 4

Ex vivo sprouting angiogenesis. (A) Quantification of neovessel outgrowth from 7-day collagen-embedded aortic rings from WT (n = 3) and *Lcn2*$^{-/-}$ (n = 3) mice. n: number of mice. (B) Representative images of aortic rings. Data were analyzed using independent sample Student's *t*-tests and are presented as mean ± SEM. **P < 0.01.

Vascular Biology (2025) **7** e250001
https://doi.org/10.1530/VB-25-0001

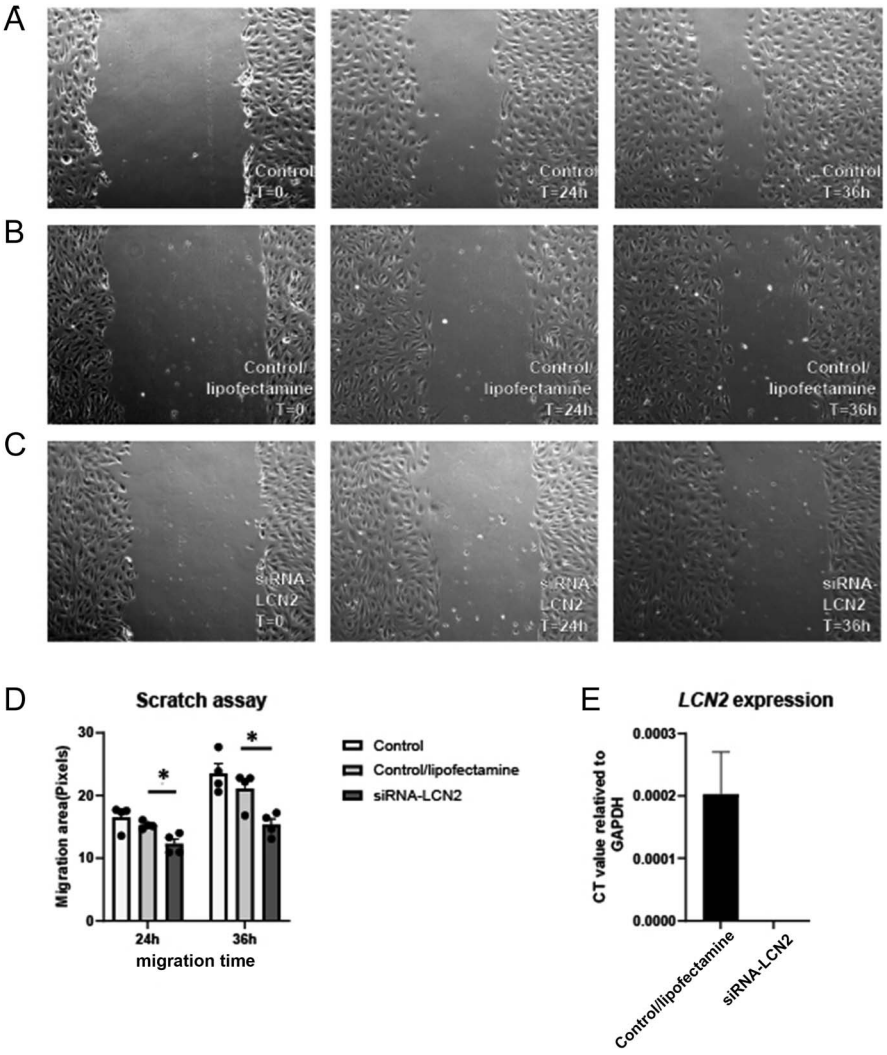

Figure 5

Scratch assay with HMVECs *in vitro*. (A) Representative images of HMVECs treated with culture medium as the control group after scratching. T: the time lag between scratching and photograph, or the migration time. (B) Representative images of HMVECs after scratching. HMVECs were treated with culture medium and lipofectamine as the control/lipofectamine group. (C) Representative images of HMVECs after scratching. HMVECs were transfected with siRNA-LCN2. (D) Quantification of migration area at 24 and 36 h after scratching. Data were analyzed with one-way ANOVA tests and presented as mean ± SEM of four independent experiments, $*P < 0.05$. (E) Quantification of LCN2 expression after siRNA-LCN2 transfection in HMVECs with RT-qPCR. Experiments were performed three times. Control/lipofectamine group: HMVECs were treated with culture medium and lipofectamine. siRNA-LCN2 group: HMVECs were transfected with siRNA-LCN2 following the protocol.

Scratch assay after LCN2 knockdown

To investigate the migration effect of *LCN2* knockdown, scratch assays were performed after siRNA transfection. The siRNA-LCN2 group showed decreased migration area compared to the control/lipofectamine group (as shown in Fig. 5D, 20% downregulated in 24 h migration area, $P = 0.013$; 27% downregulated in 36 h migration area, $P = 0.015$).

MTT assay after LCN2 knockdown

To investigate whether *LCN2* knockdown affects proliferation function, we performed an MTT assay after siRNA transfection. The value of absorbance represents the cellular proliferation/viability after different treatments. As shown in Fig. 6A, HMVECs transfected with siRNA-LCN2 did not show a difference with the control group or control/lipofectamine group.

Tube formation assay after LCN2 knockdown

To further explore the angiogenic function of *LCN2 in vitro*, we performed a tube formation assay after siRNA transfection and evaluated vasculogenesis ability by the measurement of the number of segments, the number of branches, and the total length of branches (Fig. 6B). The data showed that *LCN2* knockdown via siRNA-LCN2 transfection impaired the capillary-like formation capacity of HMVECs, which was reflected in the measurement of the number of segments with 43.8% ($P = 0.008$) decrease and the total length of branches with 27.9% decreased ($P = 0.009$) compared to the control group. In Fig. 6C, the images from the control group and the control/lipofectamine group both present a more continuous network structure than the siRNA-LCN2 group.

Discussion

In the present study, we demonstrate that *Lcn2* is upregulated after induction of ischemia in C57BL/6 mice and that *Lcn2* plays a role in angiogenesis but has no functional involvement in arteriogenesis. Microarray analysis revealed that gene expression levels of *Lcn2* were the highest significantly induced gene in C57BL/6

Vascular Biology (2025) **7** e250001
https://doi.org/10.1530/VB-25-0001

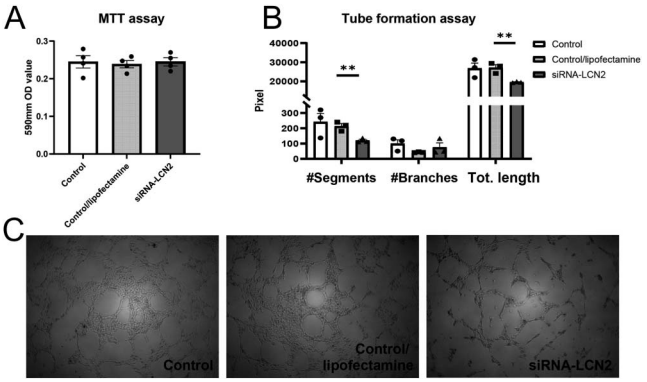

Figure 6

MTT assay and tube formation assay with HMVECs *in vitro*. (A) Quantification of HMVECs viability. HMVECs were treated with culture medium as a control group; HMVECs were treated with medium and lipofectamine as a control/lipofectamine group; HMVECs were transfected with siRNA-LCN2 as a siRNA-LCN2 group. Experiments were performed four times and results are presented as mean ± SEM. (B) Quantification of tube formation assay with HMVECs. Cells with different treatments were defined as control group, control/lipofectamine group, or siRNA-LCN2 group. #Segments, number of segments; #Branches, number of branches; Tot length, total length of branches. Experiments were performed three times. Data were analyzed with one-way ANOVA tests and presented as mean ± SEM, $^{**}P < 0.01$. (C) Representative images of tube formation assay of HMVECs transfected with siRNA-LCN2 or not.

mice 1 day after induction of HLI. Our data indicate that *Lcn2* mRNA upregulation occurs both in the adductor muscle where arteriogenesis occurs, as well as in the gastrocnemius muscle, where angiogenesis occurs upon induction of HLI. The histological evaluation of ischemic gastrocnemius after HLI showed a decreased angiogenic response in *Lcn2* knock-out mice compared to wild-type mice. In addition, in the *ex vivo* angiogenic sprouting assay, the *Lcn2* knock-out mice showed a decreased angiogenic response. Unexpectedly, we did not observe any effects on the arteriogenic response in the *Lcn2* knock-out mice after induction of HLI.

The murine HLI model is a classical method to investigate post-ischemic neovascularization, commonly employed as a model for PAD in humans (35). Previously our group published (19) that *Lcn2* is involved in atherosclerotic lesion forming and stability, which revealed the potential of *Lcn2* interference in PAD therapy. We show here that *Lcn2* deficiency leads to an impaired angiogenic response, whereas no effect on arteriogenesis was observed. Post-ischemia neovascularization is a complex process involving inflammatory and vascular cells. For example, macrophage polarization during inflammation is widely studied in neovascularization. For example, Jetten *et al.* showed in a Matrigel angiogenesis model that anti-inflammatory M2 but not pro-inflammatory M1 macrophages promote angiogenesis (36, 37). However, it was found that *Lcn2*$^{-/-}$ mice display higher expression of M1 markers and fewer M2 markers in adipose tissue and liver after a high-fat diet (38). It is highly possible that the inflammatory microenvironment of ischemic muscle in L*cn2*$^{-/-}$ mice presents a similar pattern, thus inducing *Lcn2*$^{-/-}$ mice with impaired angiogenesis ability. Hence, in ensuing investigations, the examination of the M1/M2 marker ratios within plaques of L*cn2*$^{-/-}$ mice in the HLI model will yield pivotal elucidations.

Furthermore, in vascular remodeling and angiogenesis, vascular cells such as smooth muscle cells and endothelial cells play important roles. *Lcn2* can affect both cell types, since in smooth muscle cells *Lcn2* promotes migration and collagen-1 expression (39). Whereas in endothelial cells *Lcn2* affects VEGF expression (40). VEGF reduction and less angiogenesis were found after *Lcn2* knockdown in a breast cancer cell line (41, 42). However, the regulation pathway between *Lcn2* and VEGF is still not clear. LCN2 is also related to endothelial junctional proteins ZO-1 and VE-cadherin in the study on the recovery of blood–brain barrier integrity after ischemic stroke (43). It is reported that LCN2 restored decreased expression and membrane location of ZO-1 and VE-cadherin caused by TNFα treatment, thereby resuming endothelial permeability. In our study, besides the role of *LCN2* on migration and proliferation of HMVECs, we showed the importance of *Lcn2* on endothelial cell tube formation function *ex vivo* and *in vitro* by downregulating *Lcn2* expression. Other researchers also proved that LCN2 enhanced tube formation in brain endothelial cells by adding LCN2 (27). Combining the results mentioned above, in the process of post-ischemia neovascularization, lipocalin-2 also has an effect on vascular cell function.

Angiogenesis consists of initiation, sprouting, tube formation, and vessel maturation. In this study, we confirm the importance of *Lcn2* in angiogenesis. Angiogenic sprouting assays showed fewer sprouts in aortic segments from *Lcn2* knock-out mice, suggesting that the absence of *Lcn2* hampered sprouting. With human cells, we also saw less migration in the scratch assay after siRNA transfection, indicating *LCN2* deficiency impaired cellular motility. In the tube formation assay, fewer tubes were formed after *LCN2* decreased, confirming that *LCN2* has an effect on establishing cell–cell contacts and the formation of new vessels.

Despite upregulation of *Lcn2* in adductor muscle after ischemia, our experiments showed no functional involvement in the process of arteriogenesis. Both the functional blood flow recovery and histological analysis of collateral arteries after HLI were the same in both *Lcn2*-deficient and C57BL/6 control mice. The recovery of perfusion after femoral artery ligation depends on both the extent of preexisting collaterals and collateral remodeling. In our experiments, the density of

preexisting collaterals was also no different in both strains. These results were not expected since we did see a big difference in collaterals and blood flow recovery between C57BL/6 and Balb/c mice (10, 11, 12). C57BL/6 mice obtained better angiogenesis and arteriogenesis than Balb/c mice after HLI surgery. Even though *Lcn2 expression* was significantly changed after ischemia in the adductor and gastrocnemius muscle in C57BL/6 mice, our study demonstrated that *Lcn2* was not the main contributor to arteriogenesis and collateral artery formation, but led instead to enhanced angiogenesis. These results made us question what else could drive C57BL/6 mice to recover more quickly after ischemia than Balb/c mice.

C57BL/6 and Balb/c mice are the most widely used inbred laboratory mouse strains in immune response studies. In addition to the well-documented immunological differences between C57BL/6 and Balb/c mice (44, 45, 46), there are also considerable variations in their nutritional and biochemical responses to inflammatory stimuli (47, 48). It is reasonable to assume that the higher basal level of serum total iron in Balb/c mice affects *Lcn2* upregulation. This question requires further investigation to clarify the differences in blood recovery between strains and explore the neovascularization after ischemia.

Conclusion

In this study, the role of LCN2/NGAL in neovascularization after ischemia was investigated. The results suggest that after ischemia, *LCN2* plays an important role in angiogenesis, since *LCN2* deficiency has a negative effect on angiogenesis. Surprisingly, no functional involvement of *LCN2* in the process of arteriogenesis could be demonstrated. LCN2/NGAL is a potential therapeutic target for angiogenesis induction in PAD treatment; however, the lack of effect on arteriogenesis hampers the application as an inducer for neovascularization in general in PAD.

Declaration of interest

The authors declare that there is no conflict of interest that could be perceived as prejudicing the impartiality of the research reported. P H A Quax serves as editor-in-chief of *Vascular Biology*. He was not involved in the review or editorial process for this paper, on which he is listed as an author.

Funding

This research did not receive any specific grant from any funding agency in the public, commercial, or not-for-profit sector.

Author contribution statement

All authors contributed to the study conception and design. Material preparation, data collection, and analysis were performed by LZ, ZA, HABP, and MRdV. The draft of the manuscript was written by LZ and ZA, and revised by MRdV, AYN, and PHAQ.

Acknowledgements

We thank Teun Bastiaansen and Tineke van der Pouw-Kraan for their help with the initial array analyses. We also thank Professor T W Mak of the University Health Network in Canada for kindly providing *Lcn2*$^{-/-}$ mice.

References

1 Norgren L, Hiatt WR, Dormandy JA, *et al.* Inter-society consensus for the management of peripheral arterial disease (TASC II). *J Vasc Surg* 2007 **45** (Supplement S) S5–S67. (https://doi.org/10.1016/j.jvs.2006.12.037)

2 Heil M, Eitenmuller I, Schmitz-Rixen T, *et al.* Arteriogenesis versus angiogenesis: similarities and differences. *J Cell Mol Med* 2006 **10** 45–55. (https://doi.org/10.1111/j.1582-4934.2006.tb00290.x)

3 Silvestre JS, Mallat Z, Tedgui A, *et al.* Post-ischaemic neovascularization and inflammation. *Cardiovasc Res* 2008 **78** 242–249. (https://doi.org/10.1093/cvr/cvn027)

4 van Oostrom MC, van Oostrom O, Quax PHA, *et al.* Insights into mechanisms behind arteriogenesis: what does the future hold? *J Leukoc Biol* 2008 **84** 1379–1391. (https://doi.org/10.1189/jlb.0508281)

5 Meisner JK & Price RJ. Spatial and temporal coordination of bone marrow-derived cell activity during arteriogenesis: regulation of the endogenous response and therapeutic implications. *Microcirculation* 2010 **17** 583–599. (https://doi.org/10.1111/j.1549-8719.2010.00051.x)

6 Gupta R, Tongers J & Losordo DW. Human studies of angiogenic gene therapy. *Circ Res* 2009 **105** 724–736. (https://doi.org/10.1161/circresaha.109.200386)

7 Khachigian LM, Varcoe RL, Suoranta T, *et al.* Gene therapeutic strategies for peripheral artery disease and new opportunities provided by adeno-associated virus vectors. *Arterioscler Thromb Vasc Biol* 2023 **43** 836–851. (https://doi.org/10.1161/atvbaha.122.318902)

8 Rigato M, Monami M & Fadini GP. Autologous cell therapy for peripheral arterial disease: systematic review and meta-analysis of randomized, nonrandomized, and noncontrolled studies. *Circ Res* 2017 **120** 1326–1340. (https://doi.org/10.1161/circresaha.116.309045)

9 Peeters JAHM, Schepers A, Hamming JF, *et al.* Therapeutic angiogenesis for patients with chronic limb-threatening ischemia: promising or hoax? *Vasc Biol* 2024 **6** e240009. (https://doi.org/10.1530/vb-24-0009)

10 Chalothorn D & Faber JE. Strain-dependent variation in collateral circulatory function in mouse hindlimb. *Physiol Genomics* 2010 **42** 469–479. (https://doi.org/10.1152/physiolgenomics.00070.2010)

11 van Weel V, Toes RE, Seghers L, *et al.* Natural killer cells and CD4+ T-cells modulate collateral artery development. *Arterioscler Thromb Vasc Biol* 2007 **27** 2310–2318. (https://doi.org/10.1161/atvbaha.107.151407)

12 Helisch A, Wagner S, Khan N, *et al.* Impact of mouse strain differences in innate hindlimb collateral vasculature. *Arterioscler Thromb Vasc Biol* 2006 **26** 520–526. (https://doi.org/10.1161/01.atv.0000202677.55012.a0)

13 Chalothorn D, Clayton JA, Zhang H, *et al.* Collateral density, remodeling, and VEGF-A expression differ widely between mouse strains. *Physiol Genomics* 2007 **30** 179–191. (https://doi.org/10.1152/physiolgenomics.00047.2007)

14 Nossent AY, Bastiaansen AJ, Peters EA, *et al.* CCR7-CCL19/CCL21 axis is essential for effective arteriogenesis in a murine model of hindlimb

ischemia. *J Am Heart Assoc* 2017 **6** e005281. (https://doi.org/10.1161/jaha.116.005281)

15 Kjeldsen L, Johnsen AH, Sengelov H, *et al.* Isolation and primary structure of NGAL, a novel protein associated with human neutrophil gelatinase. *J Biol Chem* 1993 **268** 10425–10432. (https://doi.org/10.1016/s0021-9258(18)82217-7)

16 Cowland JB, Sorensen OE, Sehested M, *et al.* Neutrophil gelatinase-associated lipocalin is up-regulated in human epithelial cells by IL-1 beta, but not by TNF-alpha. *J Immunol* 2003 **171** 6630–6639. (https://doi.org/10.4049/jimmunol.171.12.6630)

17 Nielsen BS, Borregaard N, Bundgaard JR, *et al.* Induction of NGAL synthesis in epithelial cells of human colorectal neoplasia and inflammatory bowel diseases. *Gut* 1996 **38** 414–420. (https://doi.org/10.1136/gut.38.3.414)

18 Flo TH, Smith KD, Sato S, *et al.* Lipocalin 2 mediates an innate immune response to bacterial infection by sequestrating iron. *Nature* 2004 **432** 917–921. (https://doi.org/10.1038/nature03104)

19 Amersfoort J, Schaftenaar FH, Douna H, *et al.* Lipocalin-2 contributes to experimental atherosclerosis in a stage-dependent manner. *Atherosclerosis* 2018 **275** 214–224. (https://doi.org/10.1016/j.atherosclerosis.2018.06.015)

20 Hemdahl AL, Gabrielsen A, Zhu C, *et al.* Expression of neutrophil gelatinase-associated lipocalin in atherosclerosis and myocardial infarction. *Arterioscler Thromb Vasc Biol* 2006 **26** 136–142. (https://doi.org/10.1161/01.atv.0000193567.88685.f4)

21 te Boekhorst BC, Bovens SM, Hellings WE, *et al.* Molecular MRI of murine atherosclerotic plaque targeting NGAL: a protein associated with unstable human plaque characteristics. *Cardiovasc Res* 2011 **89** 680–688. (https://doi.org/10.1093/cvr/cvq340)

22 Zografos T, Haliassos A, Korovesis S, *et al.* Association of neutrophil gelatinase-associated lipocalin with the severity of coronary artery disease. *Am J Cardiol* 2009 **104** 917–920. (https://doi.org/10.1016/j.amjcard.2009.05.023)

23 Sahinarslan A, Kocaman SA, Bas D, *et al.* Plasma neutrophil gelatinase-associated lipocalin levels in acute myocardial infarction and stable coronary artery disease. *Coron Artery Dis* 2011 **22** 333–338. (https://doi.org/10.1097/mca.0b013e3283472a71)

24 Saenz-Pipaon G, Ravassa S, Larsen KL, *et al.* Lipocalin-2 and calprotectin potential prognosis biomarkers in peripheral arterial disease. *Eur J Vasc Endovasc Surg* 2022 **63** 648–656. (https://doi.org/10.1016/j.ejvs.2022.01.012)

25 Liu Q & Nilsen-Hamilton M. Identification of a new acute phase protein. *J Biol Chem* 1995 **270** 22565–22570. (https://doi.org/10.1074/jbc.270.38.22565)

26 Parma L, Baganha F, Quax PHA, *et al.* Plaque angiogenesis and intraplaque hemorrhage in atherosclerosis. *Eur J Pharmacol* 2017 **816** 107–115. (https://doi.org/10.1016/j.ejphar.2017.04.028)

27 Wu L, Du Y, Lok J, *et al.* Lipocalin-2 enhances angiogenesis in rat brain endothelial cells via reactive oxygen species and iron-dependent mechanisms. *J Neurochem* 2015 **132** 622–628. (https://doi.org/10.1111/jnc.13023)

28 Berger T, Togawa A, Duncan GS, *et al.* Lipocalin 2-deficient mice exhibit increased sensitivity to Escherichia coli infection but not to ischemia-reperfusion injury. *Proc Natl Acad Sci U S A* 2006 **103** 1834–1839. (https://doi.org/10.1073/pnas.0510847103)

29 Hellingman AA, Bastiaansen AJ, de Vries MR, *et al.* Variations in surgical procedures for hind limb ischaemia mouse models result in differences in collateral formation. *Eur J Vasc Endovasc Surg* 2010 **40** 796–803. (https://doi.org/10.1016/j.ejvs.2010.07.009)

30 Zhang H, Prabhakar P, Sealock R, *et al.* Wide genetic variation in the native pial collateral circulation is a major determinant of variation in severity of stroke. *J Cereb Blood Flow Metab* 2010 **30** 923–934. (https://doi.org/10.1038/jcbfm.2010.10)

31 Bastiaansen AJ, Ewing MM, de Boer HC, *et al.* Lysine acetyltransferase PCAF is a key regulator of arteriogenesis. *Arterioscler Thromb Vasc Biol* 2013 **33** 1902–1910. (https://doi.org/10.1161/atvbaha.113.301579)

32 Bastiaansen AJ, Karper JC, Wezel A, *et al.* TLR4 accessory molecule RP105 (CD180) regulates monocyte-driven arteriogenesis in a murine hind limb ischemia model. *PLoS One* 2014 **9** e99882. (https://doi.org/10.1371/journal.pone.0099882)

33 Baker M, Robinson SD, Lechertier T, *et al.* Use of the mouse aortic ring assay to study angiogenesis. *Nat Protoc* 2011 **7** 89–104. (https://doi.org/10.1038/nprot.2011.435)

34 Scholz D, Ziegelhoeffer T, Helisch A, *et al.* Contribution of arteriogenesis and angiogenesis to postocclusive hindlimb perfusion in mice. *J Mol Cell Cardiol* 2002 **34** 775–787. (https://doi.org/10.1006/jmcc.2002.2013)

35 Krishna SM, Omer SM & Golledge J. Evaluation of the clinical relevance and limitations of current pre-clinical models of peripheral artery disease. *Clin Sci* 2016 **130** 127–150. (https://doi.org/10.1042/cs20150435)

36 Jetten N, Verbruggen S, Gijbels MJ, *et al.* Anti-inflammatory M2, but not pro-inflammatory M1 macrophages promote angiogenesis in vivo. *Angiogenesis* 2014 **17** 109–118. (https://doi.org/10.1007/s10456-013-9381-6)

37 Yang Y, Guo Z, Chen W, *et al.* M2 macrophage-derived exosomes promote angiogenesis and growth of pancreatic ductal adenocarcinoma by targeting E2F2. *Mol Ther* 2021 **29** 1226–1238. (https://doi.org/10.1016/j.ymthe.2020.11.024)

38 Guo H, Jin D & Chen X. Lipocalin 2 is a regulator of macrophage polarization and NF-kappaB/STAT3 pathway activation. *Mol Endocrinol* 2014 **28** 1616–1628. (https://doi.org/10.1210/me.2014-1092)

39 Shibata K, Sato K, Shirai R, *et al.* Lipocalin-2 exerts pro-atherosclerotic effects as evidenced by in vitro and in vivo experiments. *Heart Vessel* 2020 **35** 1012–1024. (https://doi.org/10.1007/s00380-020-01556-6)

40 Melincovici CS, Bosca AB, Susman S, *et al.* Vascular endothelial growth factor (VEGF) – key factor in normal and pathological angiogenesis. *Rom J Morphol Embryol* 2018 **59** 455–467.

41 Gote V & Pal D. Octreotide-targeted Lcn2 siRNA PEGylated liposomes as a treatment for metastatic breast cancer. *Bioengineering* 2021 **8** 44. (https://doi.org/10.3390/bioengineering8040044)

42 Guo P, Yang J, Jia D, *et al.* ICAM-1-Targeted, Lcn2 siRNA-encapsulating liposomes are potent anti-angiogenic agents for triple negative breast cancer. *Theranostics* 2016 **6** 1–13. (https://doi.org/10.7150/thno.12167)

43 Du Y, Li W, Lin L, *et al.* Effects of lipocalin-2 on brain endothelial adhesion and permeability. *PLoS One* 2019 **14** e0218965. (https://doi.org/10.1371/journal.pone.0218965)

44 Mendiola M, Tharakan A, Chen M, *et al.* Characterization of a novel high-dose ovalbumin-induced murine model of allergic sinonasal inflammation. *Int Forum Allergy Rhinol* 2016 **6** 964–972. (https://doi.org/10.1002/alr.21768)

45 de Haan N, Reiding KR, Kristic J, *et al.* The N-glycosylation of mouse immunoglobulin G (IgG)-Fragment crystallizable differs between IgG

subclasses and strains. *Front Immunol* 2017 **8** 608. (https://doi.org/10.3389/fimmu.2017.00608)

46 Fornefett J, Krause J, Klose K, *et al.* Comparative analysis of humoral immune responses and pathologies of BALB/c and C57BL/6 wildtype mice experimentally infected with a highly virulent rodentibacter pneumotropicus (pasteurella pneumotropica) strain. *BMC Microbiol* 2018 **18** 45. (https://doi.org/10.1186/s12866-018-1186-8)

47 Watanabe H, Numata K, Ito T, *et al.* Innate immune response in Th1- and Th2-dominant mouse strains. *Shock* 2004 **22** 460–466. (https://doi.org/10.1097/01.shk.0000142249.08135.e9)

48 Amini M, Nahrevanian H, Khatami S, *et al.* Biochemical association between essential trace elements and susceptibility to Leishmania major in BALB/c and C57BL/6 mice. *Braz J Infect Dis* 2009 **13** 83–85. (https://doi.org/10.1590/s1413-86702009000200002)